Analysis, design and implementation of a hybrid three-port switchable power splitter (SPWS) on Kapton flexible substrate

B. Ravelo, B Mirkhaydarov, G P Rigas, M Shkunov, S Swaisaenyakorn, P R Young, C C H Ng

Analysis, design and implementation of a hybrid three-port switchable power splitter (SPWS) on Kapton flexible substrate

B. Ravelo[1], B. Mirkhaydarov[2], G. P. Rigas[2,3], M. Shkunov[2], S. Swaisaenyakorn[4], P. R. Young[4] and C. C. H. Ng[4]

[1] Normandy University UNIROUEN, ESIGELEC, IRSEEM EA 4353, F-7600 Rouen, France

[2] Advanced Technology Institute, Electronic Engineering, University of Surrey, Guildford, Surrey, GU2 7XH, UK

[3] National Physical Laboratory (NPL), Teddington, Middlesex, TW110LW, UK

[4] School of Engineering and Digital Arts, Jennison Building, University of Kent, Canterbury, Kent, CT2 7NT, UK

E-mail: blaise.ravelo@esigelec.fr

Abstract: A topology of switchable power splitter (SPWS) ink-jet printed on flexible Kapton substrate is developed in this paper. The SPWS circuit diagram integrating a Tee PWS is described based on the synoptic approach. The complete theoretical formulations of the SPWS reflection and transmission coefficients were established. The analytical expressions enabling to assess the Tee-PWS elementary output lines for the SPWS input matching are elaborated. To validate the relevance of the proposed SPWS, a proof of concept was synthesized, designed and implemented in microstrip hybrid technology by using the packaged switch biased with 3.3 V DC supply. The fabricated circuit was directly ink-jet printed on a low cost flexible Kapton® polyimide film, using a Dimatix DMP-2831 materials printer. Then, comparisons between the experimental and electromagnetic and circuit co-simulated S-parameters from the SPWS prototype were performed. The measured SPWS performance to operate in the IEEE standard 802.11a bands from 5.4–5.7 GHz was presented. The SPWS presents overall insertion losses of about -5.5 dB and -13 dB respectively for the switches on- and off-state. Furthermore, the input and output return losses are respectively with average value of about -11 dB in the expected operation frequency band.

Keywords: Flexible electronics design, hybrid implementation, ink-jet printed technology, Kapton substrate, microwave circuit, switchable power splitter (SPWS).

I. INTRODUCTION

The printed flexible electronics constitute an emerging class of technology with potential application for microwave components [1-3]. The flexible technology offers a best tradeoff for the design of low cost ubiquitous electronic circuits [2]. In addition, the trend of the flexible electronic applications is well adapted to the needs of the ubiquitous electronic design. Among the notable spectacular growth, one can cite the explosion of the flexible technology driven by the demand of the wearable wireless body area network (WBAN) systems [4]. As reported in Figure 1 [1], the printed flexible electronics market is forecasted with an exponential growth in the next decade.

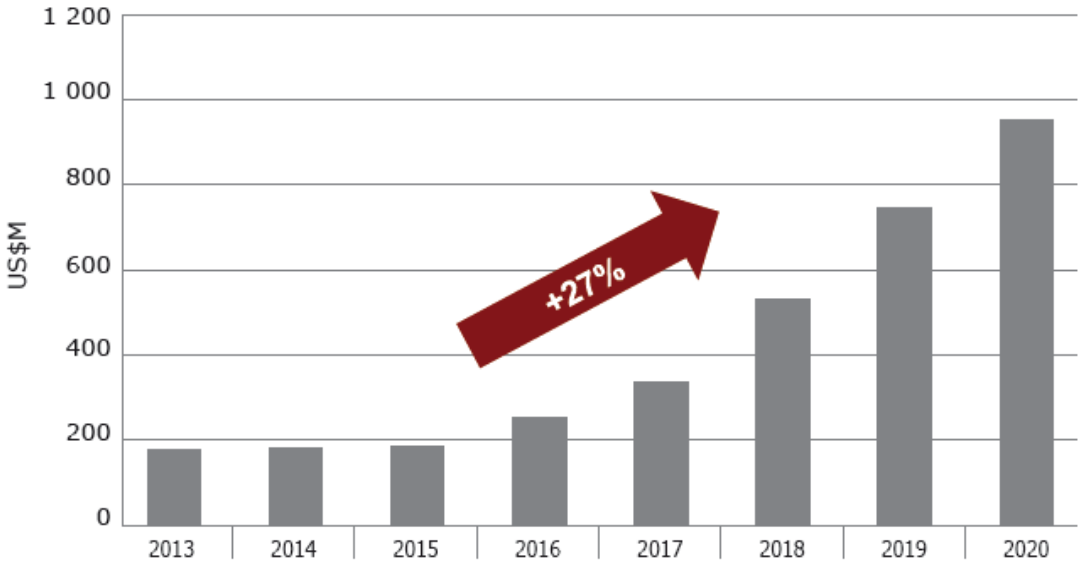

Fig. 1. Forecast on the printed & flexible electronics market [1].

Recent advances in soluble materials offer the possibility to fully print Light Emitting Diodes (LEDs), Field Effect Transistors (FETs), antennas and sensors on a variety of flexible substrates [5][6], opening the route for the realization of a plethora of new concepts such as remote medical

healthcare and the internet of things [7]. Direct inkjet printing of functionalized inks holds most of the promise for this new class of devices due to its potentials as a low cost alternative to the conventional techniques. Fast prototyping, design flexibility and large area production are some of its most notable advantages [8]. For the illustration, the photograph of the flexible microwave circuit layout investigated in this paper is presented in Figure 2.

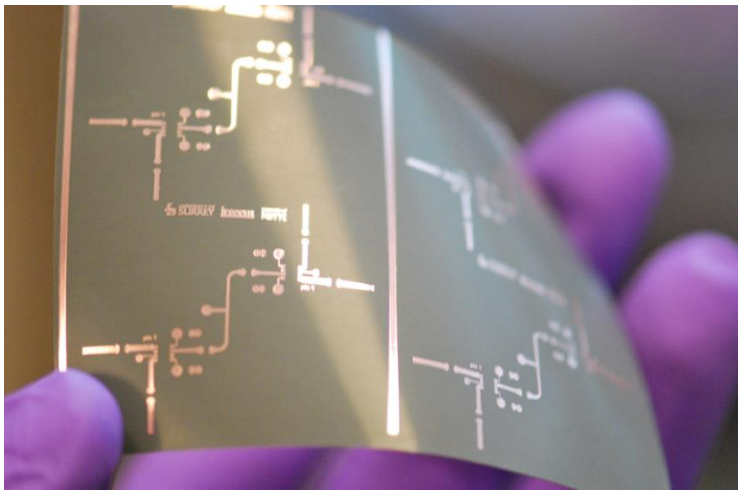

Fig. 2. Layout of the microwave circuit ink-jet printed on flexible plastic substrate under study.

Recently, prototypes of temperature sensors printed on flexible substrate were implemented [9]. In addition, complex active matrix circuits using printed organic field effect transistors were implemented on flexible substrate [10]. In the future, this emerging technology can be envisaged for the fabrication of more competitive printed electronic systems. Among the expected applications, one can envision the design of RF/microwave components for the wireless indoor communication system as Bluetooth, Wi-Fi and RFID. An example of antennas on flexible low-cost conducted inkjet-printed on paper-based substrates was proposed in [11] for RFID and WSN applications. A direct write printed antenna for the WLAN application was also designed in [12]. More recently, the feasibility of the CPW monopole [13] and dipole [14] antenna designs for the 60GHz ISM band was suggested. Furthermore, design of various topologies of classical antennas notably for the dual band operation was proposed in [15-17].

More importantly, contrary to the classical rigid planar circuit, the flexible technology offers original concepts of microwave design on plastic bendable substrates. For example, this flexibility was exploited for optimizing the directivity of the array antenna as an innovative

switched beam forming method introduced in [18]. However, for this configuration, the passive front-end circuit can present unexpected insertion losses as the case of the reconfigurable orthogonal antenna system in [19]. In upstream of the antenna, multiple way power distribution devices as the power splitters (PWSs) [20-22] can be used. So far, few investigations were performed on the design and implementation of the flexible microwave circuits as the PWS.

Thanks to the flexibility, an original complete theory and experimental investigation of a switchable PWS (SPWS) is investigated in this paper. This research work is the expansion of the results published in [23]. The SPWS microwave circuit proof of concept (POC) design and implementation on flexible Kapton substrate will be described. In addition to the results presented in [23], the analytical theory will be established in Section II. Then, discussions of simulated and experimental results will be presented in Section III. The conclusion of the paper will be drawn in Section IV.

II. ANALYTICAL INVESTIGATION ON THE PROPOSED THREE PORT SPWS

The SPWS topology under study is assumed as a multi-way microwave network with 1-port input and 4-port output terminals. It acts as an electrical single-input multiple-output (SIMO) system. To operate as PWS, the pair of outputs can be selected alternatively with binary control voltages V_{CTL} sets to logic state “1” or “0” respectively corresponding to V_0 and GND. After the description of the topology, analytical investigation enabling to determine the SPWS reflection and transmission coefficients will be developed.

A. Topological Concept of the Proposed Flexible SPWS

The proposed SPWS topology can be assumed as a tree port microwave circuit. The two of five ports are in off-state in normal operation. As introduced in [23], the proposed SPWS will be designed in planar technology as shown in top of Figure 3.

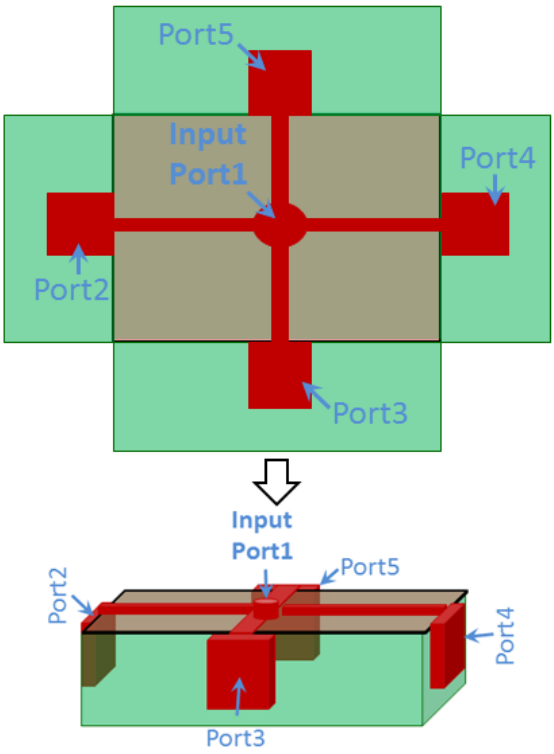

Fig. 3. Configuration of the SPWS structure (top: planar design; bottom: perspective view).

In practice, 1-port input and 2-ports output way PWS can be used to design this SPWS topology. The SPWS input (Port ①) is placed at the center of the structure and the outputs (Port ②-⑤) are set symmetrically in the four different directions. Then, the 3D configuration can be established from planar design. An example of perspective view is introduced in bottom of Figure 3. Thanks to the flexibility property, the planar circuit can be envisaged to be folded to realize this 3D concept.

As depicted in Figure 4, the SPWS topology is essentially composed of Tee-PWS whose output branches are terminated by the two switches. To select alternatively the targeted output, two switches will be integrated between each output branches of the PWS. Figure 4 represents the SPWS synoptic diagram.

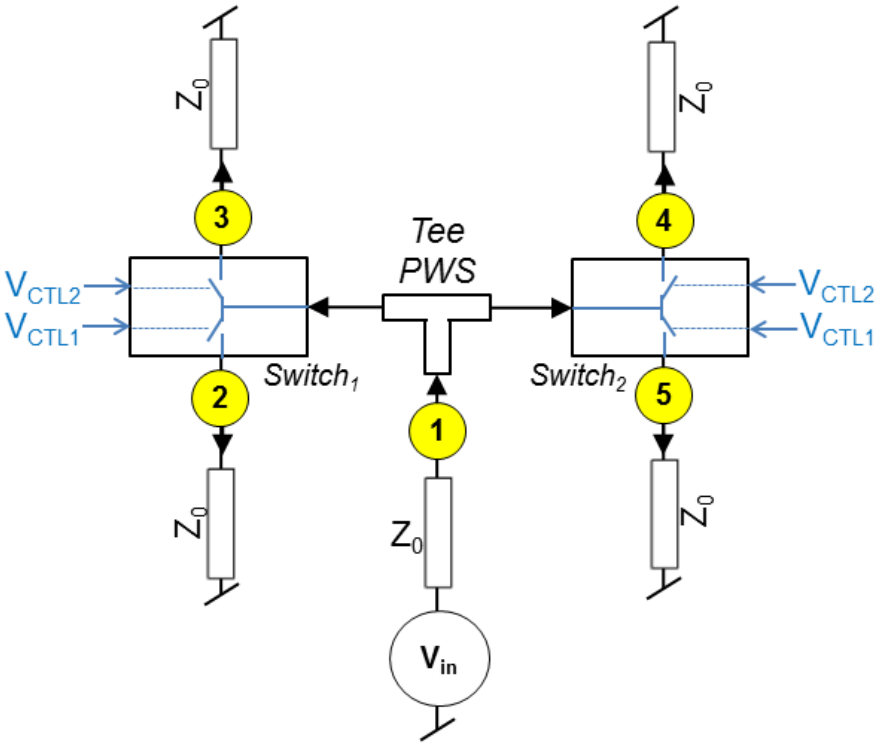

Fig. 4. Configuration of the SPWS structure (top: planar design; bottom: perspective view) and (b) synoptic diagram of the SPWS topology under study.

Similar to all classical RF/microwave devices, the proposed SPWS circuit is intended to operate with the standard reference load impedance Z_0=50Ω. As expressed in Figure 2(b), in the normal functioning, the input signal is injected at port ①. Then, it will be in turn subdivided into output signals terminated by ports ②, ③, ④ and ⑤. The two switches are fed by the control and also bias voltages V_{CTL1} or alternatively V_{CTL2}. These control supply can be attributed to 0V in "off-state" (logic state "0") or V_0 in "on-state" (logic state "1"). To choose the configurations depend on the combination of the activated control voltages V_{CTL1} and V_{CTL2}. As illustrated in Table I, $Switch_1$ and $Switch_2$ are expected to operate in two alternative configurations of:

- **Status A** represented by "②←①→④" means that the signal inputted from ① is splitted simultaneously into Outputs ② and ④,
- **Status B** represented by "③←①→⑤" means that the signal inputted from ① is splitted simultaneously into Outputs ③ and ⑤.

The truth table illustrating the operation principle of the SPWS is addressed in Table I. The "on-state" corresponds to the feeding DC voltage V_0. Thus, inversely, if the control voltage V_{CTL}=0 and if the switch is in "off-state". Therefore, in the ideal case, the transmission parameters corresponding to the off-state output port are ideally zero.

TABLE I

TRUTH TABLE OF THE SPWS SHOWN IN FIG. 1

SPWS status	**Switch$_1$**	**Switch$_2$**	**Ideal transmission parameters**
STATUS A	$V_{CTL1}=V_0$, $V_{CTL2}=0$	$V_{CTL1}=0$, $V_{CTL2}=V_0$	$S_{31}=0$ $S_{51}=0$
STATUS B	$V_{CTL1}=0$, $V_{CTL2}=V_0$	$V_{CTL1}=V_0$, $V_{CTL2}=0$	$S_{21}=0$ $S_{41}=0$

In practice, the Tee of the SPWS must be constituted by realistic microstrip transmission lines (TLs). Based on the microwave and TL theory, the S-parameter expressions of the elementary TL can be expressed naturally knowing their physical parameters. By this way the theoretical approach enabling to establish the SPWS S-parameters will be described in the next paragraph.

B. Mathematical Synthesis of the SPWS S-Parameters

The present analytical investigation is fundamentally drawn from the equivalent circuit diagram of the SPWS shown in Figure 5. This system can be represented as a SIMO network. In the ideal case, Switch$_1$ and Switch$_2$ are assumed to be analytically identical. Therefore, the path Input-Output$_1$ and Input-Output$_2$ are also electrically identical.

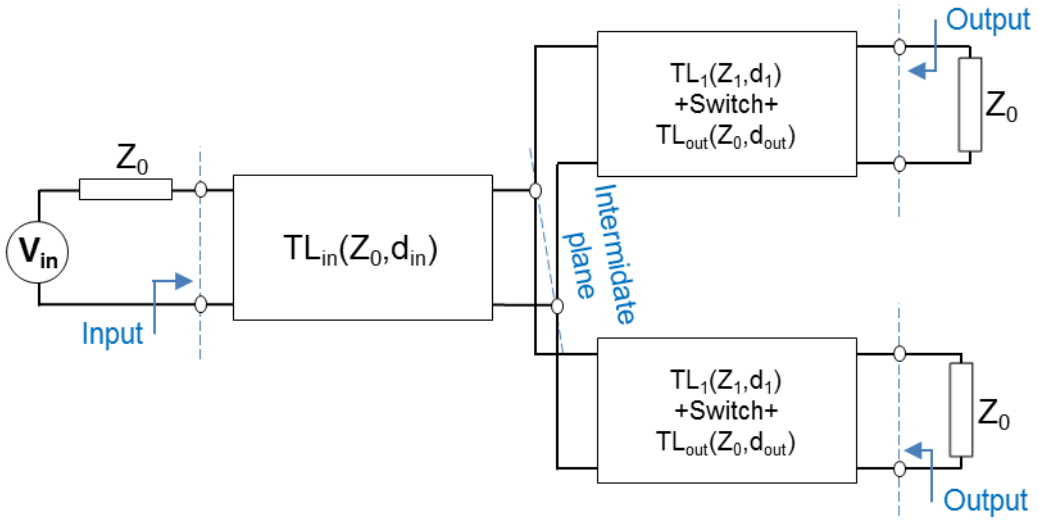

Fig. 5. Functional operational system of the SPWS - (b) Equivalent circuit of the SPWS topology composed of elementary TLs and the switch black box - (c) The electrical chain of the output blocks.

After the S-to-Y matrix transform and the output branch Y-matrices addition, the electrical equivalent as single-input single-output (SISO) network can be established. Figure 6(a) highlights the configuration of the SISO equivalent diagram. Subsequently, the global S-parameter model is determined from the product of the ABCD matrices which models mathematically to the cascaded two elementary blocks TL_{in} and $[S]_{out}$. It can be emphasized in Figure 6(b) that the proposed SPWS model should include the switch black box denoted $[S]_{switch}$.

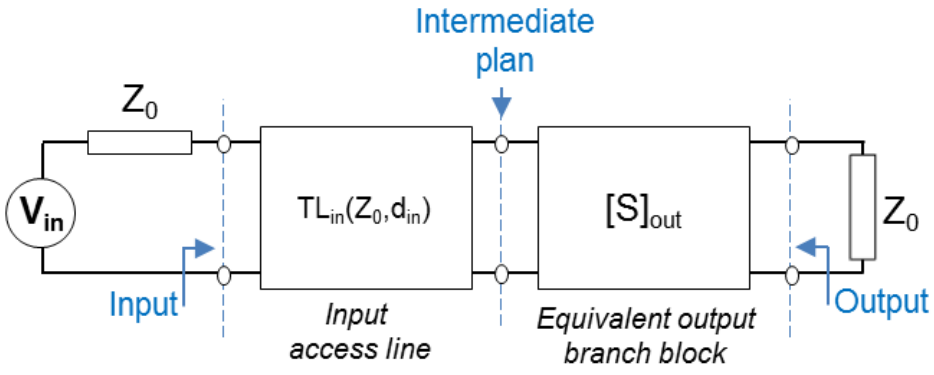

(a)

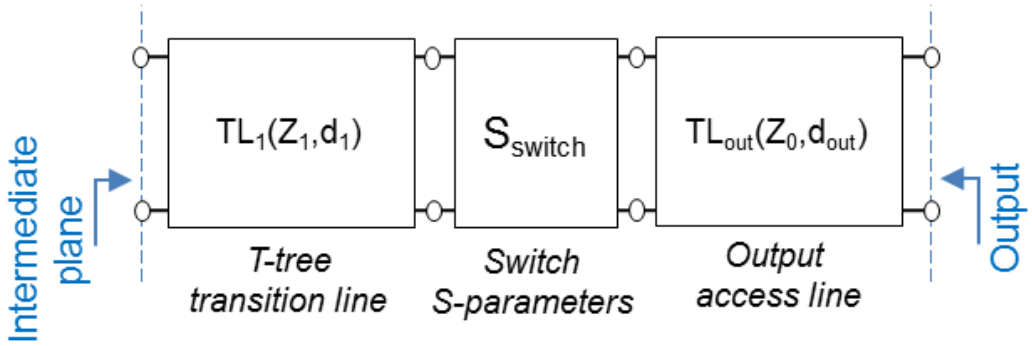

(b)

Fig. 6. (a) Equivalent circuit of the SPWS topology composed of elementary TLs and the switch black box and (b) equivalent output blocks.

It is worth noting that in this paper, each TL represented by TL(Z_c,d) is characterized by their characteristic impedance Z_c and their electrical length $\theta=\beta\times d$. It can be reminded that the physical length, d and the phase constant, β. As described in the previous paragraph, the PWS is considered built in distributed T-tree interconnect topology. Consequently, the elementary lines of the tree can be assumed constituted by the input access line $TL_{in}(Z_0,d_{in})$ (with characteristic impedance Z_0 and physical length d_{in}) and two identical transition lines $TL_1(Z_1,d_1)$. The output access lines are designated by $TL_{out}(Z_0,d_{out})$ as can be understood in Figures 3. As introduced in [24], the corresponding S-parameters are expressed as:

$$[S]_{TL}=\begin{bmatrix} S_{11TL} & S_{12TL} \\ S_{21TL} & S_{22TL} \end{bmatrix}, \tag{1}$$

with

$$S_{11TL}=S_{22TL}=\frac{\sin(\theta)(Z_c^2-Z_0^2)}{(Z_0^2+Z_c^2)\sin(\theta)+2Z_0Z_c\cos(\theta)}, \tag{2}$$

$$S_{12TL}=S_{21TL}=\frac{2Z_0Z_c}{(Z_0^2+Z_c^2)\sin(\theta)+2Z_0Z_c\cos(\theta)}. \tag{3}$$

The input and output access lines are supposed perfectly matched to Z_0 and having physical lengths d_{in} and d_{out}. The corresponding electrical lengths are respectively denoted θ_{in} and θ_{out}. By supposing the switches are identical and as a unilateral two-port network ($S_{12switch}\approx 0$), the

equivalent S-parameter can be expressed as:

$$[S]_{switch} = \begin{bmatrix} r_{11} & 0 \\ t & r_{22} \end{bmatrix}. \tag{4}$$

The switch reflection parameters are denoted r_{11} and r_{22}. Hence, the transmission parameter is denoted t. The S-parameters of the overall chain between the input and output branches of the SPWS are written as:

$$[S]_{SPWS} = \begin{bmatrix} S_{11SPWS} & S_{12SPWS} \\ S_{21SWPS} & S_{22SPWS} \end{bmatrix}, \tag{5}$$

with the complete expressions of the reflection and transmission parameters are:

$$S_{11SPWS} = \frac{\begin{bmatrix}\cos(\theta_1) - \sin(\theta_1)\end{bmatrix}\left\{\begin{bmatrix}((Z_1^2 + 2Z_0^2)\sin(\theta_{in}) \\ -3Z_0 Z_1 \cos(\theta_{in}))r_{11} \\ -(Z_1^2 + 2Z_0^2)\sin(\theta_{in}) + Z_0 Z_1 \cos(\theta_{in})\end{bmatrix}\right\}}{\begin{bmatrix}\cos(\theta_1) + \sin(\theta_1)\end{bmatrix}\left\{\begin{bmatrix}((Z_1^2 - 2Z_0^2)\sin(\theta_{in}) \\ +Z_0 Z_1 \cos(\theta_{in}))r_{11} \\ -(Z_1^2 + 2Z_0^2)\sin(\theta_{in}) - 3Z_0 Z_1 \cos(\theta_{in})\end{bmatrix}\right\}}, \tag{6}$$

$$S_{21SPWS} = \frac{8Z_0 Z_1 t}{\begin{bmatrix}\cos(\theta_1) + \sin(\theta_1)\end{bmatrix}\left\{\begin{bmatrix}3\cos(\theta_{out}) + 3\sin(\theta_{out}) \\ +(\sin(\theta_{out}) - \cos(\theta_{out}))r_{22}\end{bmatrix}\right.} \\ \left.\begin{bmatrix}(Z_1^2 + 2Z_0^2)\sin(\theta_{in}) - 3Z_0 Z_1 \cos(\theta_{in}) \\ -((Z_1^2 - 2Z_0^2)\sin(\theta_{in}) + Z_0 Z_1 \cos(\theta_{in}))r_{11}\end{bmatrix}\right\}, \tag{7}$$

$$S_{22SPWS} = \frac{\begin{bmatrix}3\left[\cos(\theta_{out}) - \sin(\theta_{out})\right]r_{22} - \sin(\theta_{out}) \\ -\cos(\theta_{out})\end{bmatrix}}{\begin{bmatrix}\left[\sin(\theta_{out}) - \cos(\theta_{out})\right]r_{22} + 3\sin(\theta_{out}) \\ +3\cos(\theta_{out})\end{bmatrix}}. \tag{8}$$

To realize the inter-stage matching at the node of the T-tree (S_{11out}=0), the characteristic

impedance of the intermediate transition line TL_1 must be expressed as:

$$Z_1 = Z_0 \frac{3r_{11} - 1 + \sqrt{\left[9 - 8\tan^2(\theta_{in})\right] r_{11}^2 - 6r_{11} + 1 + 8\tan^2(\theta_{in})}}{2(r_{11} - 1)\tan(\theta_{in})}. \quad (9)$$

Based on this relation, the SPWS matching can be analytically predicted. The trivial case $\theta_{in}=0$ implies $Z_1=\infty$. As a graphical illustration, Figure 7 displays the variation of the ratio $|Z_1|/Z_0$ in dB versus the electrical length θ_{in} and the reflection coefficient r_{11}. It can be pointed out that the characteristic impedance Z_1 increases with r_{11}. Moreover, Z_1 can vary up to about 320 times the reference impedance Z_0 when the electrical length θ_{in} is increased.

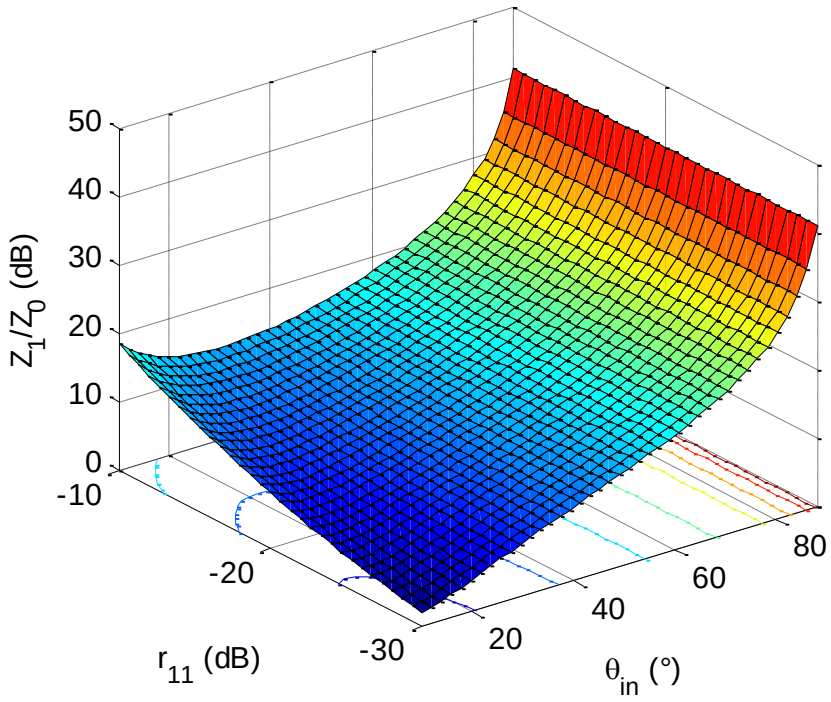

Fig. 7. Variation of the transition line characteristic impedance $|Z_1|/Z_0$ vs (θ_{in}, r_{11}).

To validate the relevance of the SPWS concept under investigation, design and fabrication results of the demonstrator will be introduced and discussed in the following section.

III. DESIGN AND VALIDATIONS OF THE 3-PORT SPWS PROOF-OF-CONCEPT

As a POC of the SPWS, a microwave circuit prototype was synthesized and fabricated. For that, a novel fabrication process of microstrip circuit on flexible plastic was deployed. The SPWS was innovatively implemented in hybrid technology ink-jet printed on the flexible Kapton substrate. To validate the POC, simulations and measurements were performed. It is worth emphasizing that the electromagnetic (EM) and circuit co-simulations presented in this paper were run in the ADS/Momentum environment from Keysight technologies®.

A. Design and Implementation of the Proposed SPWS Prototype

An active circuit was designed and implemented in hybrid microstrip technology as the demonstrator. As dielectric substrate, an h=152 µm thick Kapton® polyimide film with a t=18 µm Cu lamination at both sides was used. The circuit layout was patterned on top of the one side, by depositing a 300 nm thin film of poly-methyl-methacrylate (PMMA) using a Fujifilm DMP-2831 materials ink-jet printer. The PMMA film acted as a protective layer during the Cu etching process, revealing the conductive tracks with a conductivity of about 8.54 MS/m.

Based on these parameters, the POC of SPWS was synthesized, optimized and designed. The mask and the photograph of the fabricated SPWS is displayed in Figure 8(a) and Figure 8(b). The fabricated circuit physical size is 34 mm × 28 mm. The fabricated SPWS is integrating the packaged SKY13298-360LF GaAs switch. The bias voltage is V_0 = 3.3V DC supply which corresponds to the on-state. Based on the technical characteristics provided by the manufacturer, it presents isolation from -0.4 dB to -1 dB and isolation parameter better than -25 dB in the IEEE standard 802.11a bands. As aforementioned in Subsection II-A, in on-state, the control voltage is V_{CTL}=V_0 and the off-state corresponds to V_{CTL}=0 V.

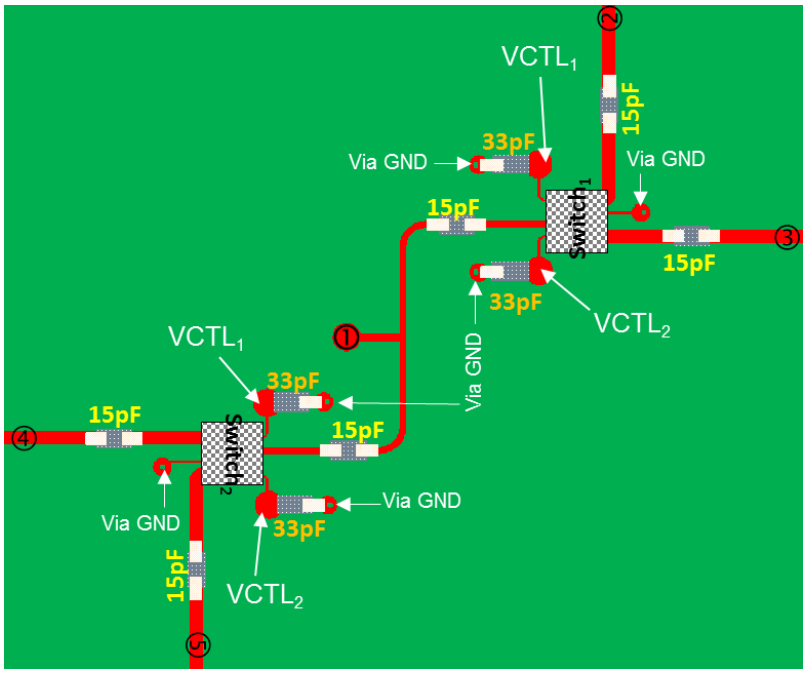

(a)

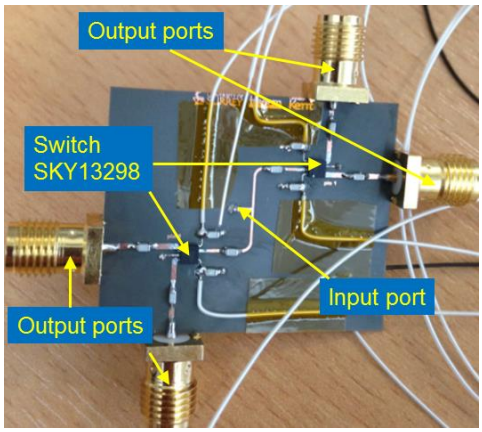

(b)

Fig. 8(a). Layout and (b) photograph of the SPWS POC implemented using hybrid technology.

Lumped isolator SMC capacitors with nominal values 15 pF and 33 pF were mounted for the decoupling between the DC and microwave signals. The distributed Tee PWS was synthesized to operate in the WLAN IEEE standard 802.11a bands defined with the centre frequency 5. 6GHz and bandwidth of about 0.4 GHz. It acts as symmetrical devices with balanced outputs implemented in microstrip hybrid technology. The EM and circuit co-simulations including the distributed transition microstrip lines and the lumped components were realized.

B. Dielectric Characterization of the Kapton Substrate Employed to Fabricate the SPWS

In order to fit the EM and circuit co-simulations of the prototype, characterization of the Kapton dielectric substrate was performed.

The characterization of the Kapton flexible substrate was practically carried out via the measurements of S-parameters. The Kapton dielectric characteristics were extracted based on the Bahl and Trivedi theory. The photograph of the microstrip TL sample is depicted in Figure 9(a). This test line presents physical length of about 14 mm.

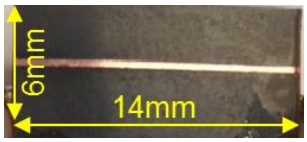

(a)

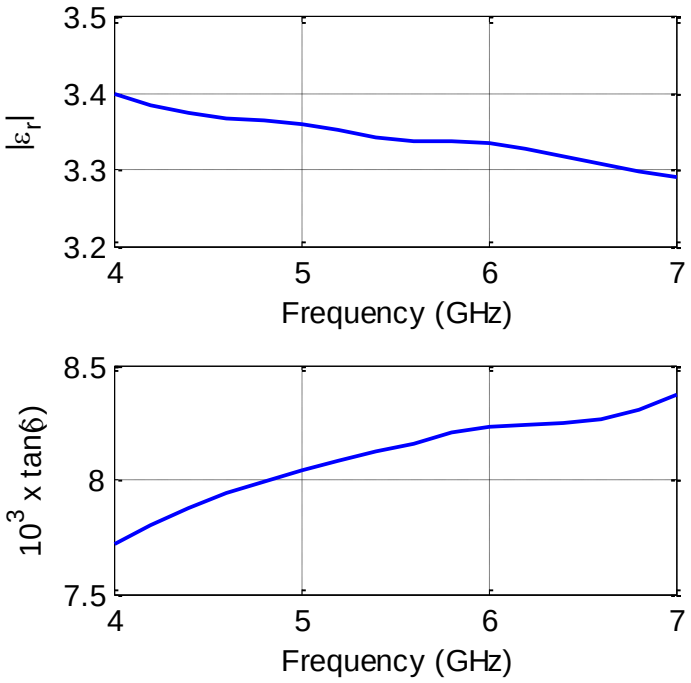

(b)

Fig. 9(a). Photograph of the microstrip TL used for the implemented circuit Kapton substrate characterization, and (b) extracted relative permittivity and tangent loss.

The frequency dependent characteristics of Kapton relative permittivity and loss tangent are plotted in Figure 9(b). It can be emphasized that the relative permittivity is dispersive at 3.3-3.4 in the frequency band 4-7 GHz. Furthermore, the Kapton loss tangent presents an average value of about 0.008. This range of value of frequency dependent extracted characteristics was considered during the EM and circuit co-simulations of the designed SPWS.

C. Comparison between Simulations and Measurements

The electrical equivalent model of the circuit displayed in Figure 8(a) was co-simulated by considering the schematic and momentum EM environments. The S-parameter model of the SKY13298-360LF GaAs switch provided by the manufacturer was integrated in the simulated circuit. Then, S-parameter measurements were made by using the Agilent VNA 8502C. The simulations and measurements of the SPWS prototype were run essentially from 5.4 GHz to 5.8 GHz.

Two configurations based on the different statuses of the switches as summarized in Table I were considered during the simulations. A good agreement between the SPWS out-branches were realized. For the simplicity, the results only through output terminals ② and ③ are examined in this paper. In Status A, we have the configurations Switch_1($V_{CTL1}=V_0$ and $V_{CTL2}=0$ V) and Switch_2($V_{CTL1}=0$ V and $V_{CTL2}=V_0$). Then, in Status B, the alternative configuration was applied. Then, the S-parameters S_{11}, S_{21}, S_{31}, S_{23}, S_{32}, S_{41}, S_{51}, S_{22}, S_{33}, S_{44} and S_{55} were visualized from 5.4 GHz to 5.8 GHz. As can be seen in Figure 10(a) and Figure 10(b), the experimental results uphold a transmission parameter of about -6 dB along the on-state output branch and -13 dB along the off-state output branch.

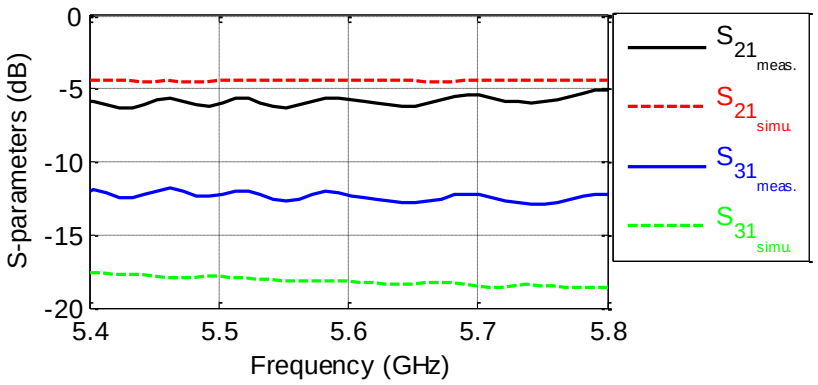
0
-5
-10
-15
-20
S-parameters (dB)
5.4
5.5
5.6
5.7
5.8
Frequency (GHz)
S21meas.
S21simu.
S31meas.
S31simu.

(a)

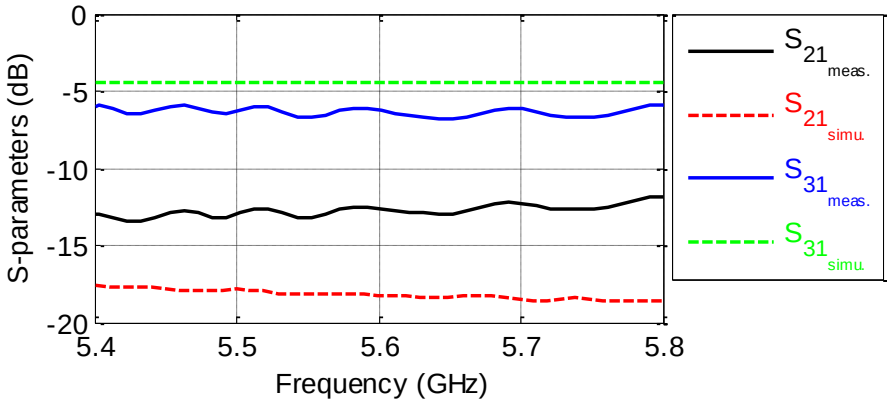
0
-5
-10
-15
-20
S-parameters (dB)
5.4
5.5
5.6
5.7
5.8
Frequency (GHz)
S21meas.
S21simu.
S31meas.
S31simu.

(b)

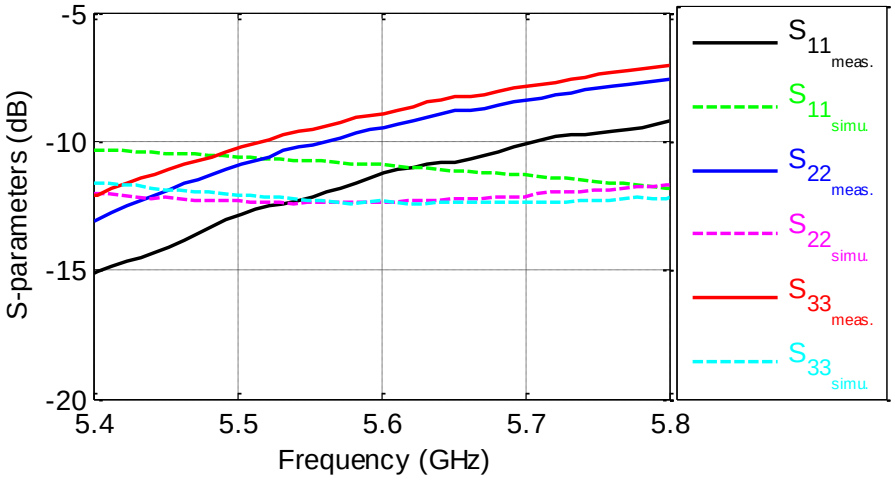
-5
-10
-15
-20
S-parameters (dB)
5.4
5.5
5.6
5.7
5.8
Frequency (GHz)
S11meas.
S11simu.
S22meas.
S22simu.
S33meas.
S33simu.

(c)

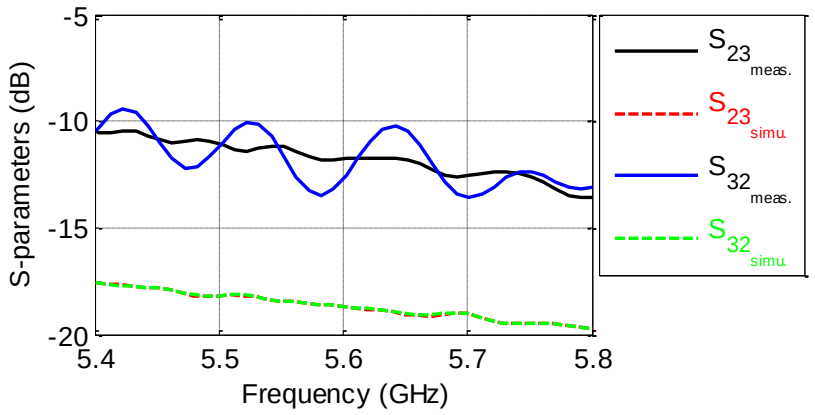

(d)

Fig. 10. Comparison of the transmission parameters of the fabricated SPWS in (a) Status A and (b) in Status B - Comparison of the measured and simulated (c) input and output reflection and (d) isolation parameters of the fabricated SPWS in both status A & B.

Due to the symmetry of the SPWS topology output branches, a good correlation between the S-parameters $S_{2,k}$ vs $S_{3,k}$ and $S_{4,k}$ vs $S_{5,k}$ (k={1,2,3,4,5}) was observed during the tests with Status A and Status B. The slight differences between the simulations and measurements are essentially due to the biasing condition of the switches which do not fit the model used during the simulations. Moreover, in the two statuses under consideration, similar results were found for the reflection and isolation coefficients through the three terminals of the SPWS. As can be seen in Figure 10(c), the average values of these coefficients in the expected frequency band are experimentally closely of about -10 dB. Due to the fabrication and measurement inaccuracies, a deviation of about 7 dB was found between the simulations and experimental results. Thanks to the unilateral aspect of the switches ($S_{12switch}$≈0), the implemented SPWS exhibits excellent inter-branch isolations.

D. Proposed SPWS Sensitivity Analyses vs Intermediate Transition Line Characteristic Impedance

In complementary to the sensitivity analysis investigation conducted in [21], the influence of the T-output lines characteristic impedance was carried out. For the further insight on the

influence of the intermediate line TL_1 defined in Figure 4(c), sensitivity analyses of the reflection and transmission parameters were carried out for Z_1 increased from 50 Ω to 60 Ω. To do this, the TL_1 width was varied based on Monte Carlo numerical analyses from 0.25 mm to 0.35 mm. Then, the SPWS S-parameters were recorded under the two configurations corresponding to Status A and Status B. Figures 11 illustrate how the SPWS S-parameters are influenced by ΔZ_1.

Figure 11(a) presents the influence of the Z_1 variation on the SPWS input reflection coefficients. It can be underlined that the input reflection coefficient varies of about 4 dB. Then, Figure 11(b) materializes that the transmission parameter is notably less sensitive to Z_1 with variation of less than 2.5 dB. The same for the output reflection losses, the variations are less than 2.5 dB for all the output terminals of the implemented hybrid SPWS.

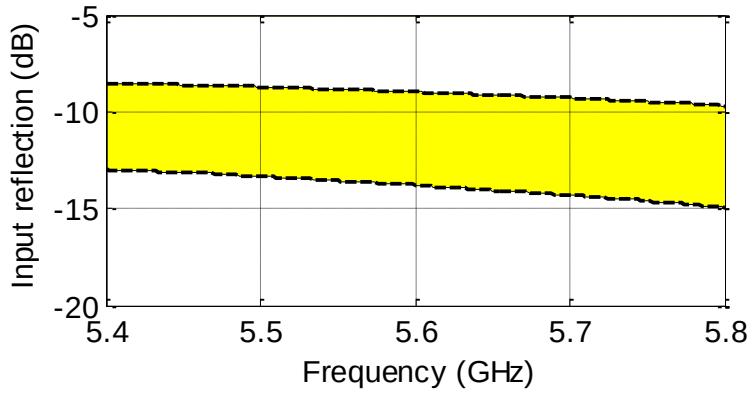

(a)

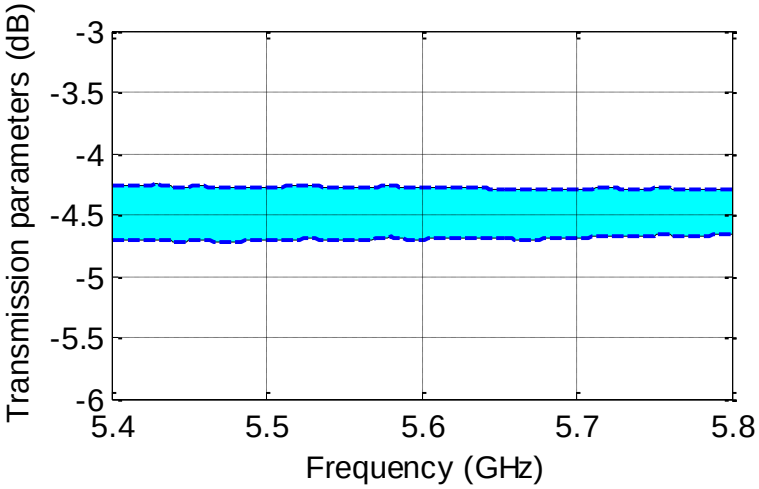

(b)

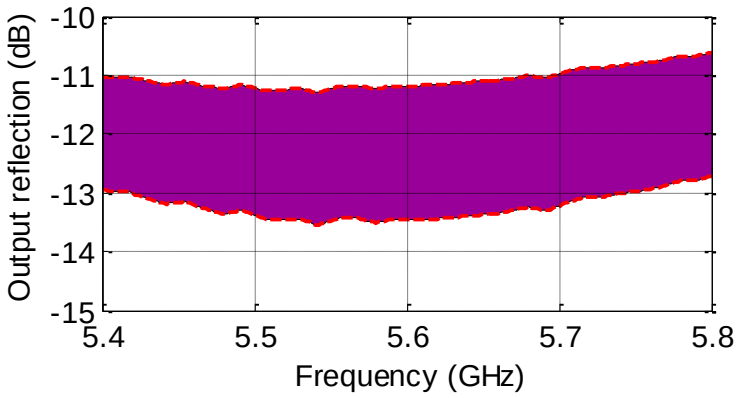

(c)

Fig. 11. SPWS Monte Carlo sensitivity analysis results: (a) input reflection, (b) transmission and (c) output reflection coefficients when Z_1 varied from 50 Ω to 60 Ω.

4. CONCLUSION

A prototype of SPWS microwave circuit is fully investigated. In addition to the work published in [23], the complete theoretical approach on the topology of the SPWS by considering a T-tree PWS is presented. The innovative concept of the SPWS topology to operate as a tree-port circuit is described. The fundamental mathematical expressions of the SPWS S-parameters in function of the elementary line and used switch parameters are established.

The prototype of the SPWS was synthesized, designed, simulated and optimized. The demonstrator was innovatively implemented on flexible Kapton substrate in hybrid ink-jet printed technology. The relevance of the SPWS circuit is verified with a POC designed and implemented on Kapton flexible substrate. The POC is composed of Tee PWS and commercial GaAs switches. Then, EM and circuit co-simulations are compared with the experimental results. Despite the deviation between the model and measured switch bias voltage characteristics, a good agreement between both results is globally observed. The S-parameter analyses are carried out in the IEEE standard 802.11a from 5.4GHz to 5.8GHz band. In addition, sensitivity analyses based on the Monte Carlo approach are also provided for the SPWS reflection and transmission coefficients. These sensitivity analyses were essentially conducted in function of the intermediate transition line between the characteristic impedance of the T-tree and the switches.

As ongoing research, the developed SPWS device can be potentially used for the low cost switched beam forming antenna system. With the subsequent capacity of the mechanical bending, the developed SPWS can be used to design of the communicating ubiquitous electronic as WBAN devices.

Acknowledgement: Acknowledgement is made to the Normandy Region for the BRIDGE (« Plateforme transversale de recherche entre les Bandes optiques et Radioélectriques : Intégrité du signal et de la puissance / Détection et détecteurs / Génération Electromagnétique ultra-brève et intense ») project support of this research work through the ERDF fund.

REFERENCES

[1] E. Mounier, A. Bonnabel and M. Rosina, "Flexible & Printed Electronics: Flexible Applications Based on Printed Electronics Technologies," Market & Technology Report, Yole Développement, Apr. 2013.

[2] S. R. Forrest, "The Path to Ubiquitous and Low-Cost Organic Electronic Appliances on Plastic," Nature, vol. 428, Apr. 2004, pp. 911-918.

[3] European Project FP7 Programme, "Commercialising Organic and Large Area Electronics," [Online]. Available: http://www.colae.eu/, Accessed 2014.

[4] K. M. S. Thotahewa, J.-M. Redoute and M. R. Yuce, "A Low-Power Wearable Dual-Band Wireless Body Area Network System: Development and Experimental Evaluation," IEEE Trans. MTT, vol. 62, no. 12, Dec. 2014, pp. 2954-2964.

[5] Corning, "The Emerging Innovations Group Connects Corning's Extraordinary Materials," [Online]. Available: http://www.corning.com/displaytechnologies/en/products/flexible.aspx, Accessed 2014.

[6] A. Russo, B. Y. Ahn, J. J. Adams, E. B. Duoss, J. T. Bernhard and J. A. Lewis, "Pen-on-Paper Flexible Electronics," Advanced Materials, vol. 23, no. 30, Aug. 2011, pp. 3426-3430.

[7] D. Miorandi, S. Sicari, F. De Pellegrini, and I. Chlamtac, "Internet of Things: Vision, Applications and Research Challenges," Ad Hoc Networks, vol. 10, Sept. 2012, pp. 1497-1516.

[8] A. C. Arias, S. E. Ready, R. Lujan, W. S. Wong, K. E. Paul, A. Salleo, M. L. Chabinyc, R. Apte, R. A. Street, Y. Wu, P. Liu and B. Ong, "All Jet-Printed Polymer Thin-Film Transistor Active-Matrix Backplanes," Applied Physics Letters, vol. 85, Oct. 2004, pp. 3304-3306.

[9] A. Aliane, V. Fischer and R. Coppard, "Large Area Printed Temperature Sensors on Flexible Substrate," Proc. 5th IEEE Int. Workshop on Advances in Sensors and Interfaces (IWASI), Bari, Italy, 13-14 June 2013, pp. 188-192.

[10] M. Charbonneau, S. Jacob, M. Benwadih, J. Bablet, V. Fischer, D. Boutry, R. Coppard, I. Chartier, S. Abdinia, E. Cantatore, G. Maiellaro, E. Ragonese, G. Palmisano and R. Gwoziecki, "Printed Organic TFTs for Interfacing Circuits and Active Matrix," Proc. 20th Int. Disp. Workshops (IDW'13), Sapporo, Japan, 4-6 Dec. 2013.

[11] A. Rida, L. Yang, R. Vyas and M. M. Tentzeris, "Conductive Inkjet-Printed Antennas on Flexible Low-Cost Paper-Based Substrates for RFID and WSN Applications," IEEE Ant. Prop. Mag., vol. 5, no. 3, 2009, pp. 13-23.

[12] D. E. Anagnostou, A. A. Gheethan, A. K. Amert and K. W. Whites, "A Direct-Write Printed Antenna on Paper-Based Organic Substrate for Flexible Displays and WLAN Applications," J. Disp. Technol., vol. 6, no. 11, Nov. 2010, pp. 558-564.

[13] A. Bisognin, J. Thielleux, Wei Wei, D. Titz, F. Ferrero, P. Brachat, G. Jacquemod, H. Happy and C. Luxey, "Inkjet Coplanar Square Monopole on Flexible Substrate for 60-GHz Applications," IEEE Antennas and Wireless Propagation Letters, vol. 13, 2014, pp. 435-438.

[14] K. Hettak, A. Petosa and R. James, "Flexible Plastic-Based Inkjet Printed CPW Fed Dipole Antenna for 60 GHz ISM Applications," Proc. of IEEE Ant. and Prop. Society Int. Symp. (APSURSI), 2014, Memphis, TN, 6-11 July 2014, pp. 328-329.

[15] H.-Y. Chien, C.-Y.-D. Sim and C.-H. Lee, "Compact Size Dual-band Antenna Printed on Flexible Substrate for Wlan Operation," Proc. Int. Symp. on Antennas and Propagation (ISAP), 2012, Nagoya, Japan, 29 Oct. – 2 Nov. 2012, pp. 1047-1050.

[16] A. C. Durgun, M. S. Reese, C. A. Balanis, C. R. Birtcher, D. R. Allee and S. Venugopal, "Design, Simulation, Fabrication and Testing of Flexible Bow-Tie Antennas," IEEE Trans. Ant. Prop., Vol. 59, No. 12, Dec. 2011, pp. 4425-4435.

[17] H. R. Khaleel, H. M. Al-Rizzo and A. I. Abbosh, "Design, Fabrication, and Testing of Flexible Antennas," Intech Open Book, Advancement in Microstrip Antennas with Recent Applications, Chap. 5, Ed. by A. Kishk, Mar. 2013, pp. 363-383.

[18] N. M. Jizat, S. K. A. Rahim and T. A. Rahman, "Dual Band Beamforming Network Integrated with Array Antenna", Proc. 4th Asia Int. Conf. on AMS, Kota Kinabalu, Malaysia, 26-28 May 2010, pp. 561-566.

[19] M. T. Ali, T. A. Rahman, M. R. Kamarudin, and M. N. Md Tan, "A Reconfigurable Orthogonal Antenna Array (ROAA) for Scanning Beam at 5.8GHz," Proc. Asia-Pacific Microwave Conference (APMC) 2010, Yokohama, Japan, 7-10 Dec. 2010, pp. 646-649.

[20] B. Ravelo, "Synthesis of N-Way Active Topology for Wide-Band RF/Microwave Applications," Int. J. Electronics, May 2012, pp. 597-608.

[21] Pei-Ling Chi and Kuan-Lin Ho, "Design of Dual-Band Coupler with Arbitrary Power Division Ratios and Phase Differences," IEEE Trans. MTT, vol. 62, no. 12, Dec. 2014, pp. 2965-2974.

[22] Hee-Ran Ahn, "Compact CVT-/CCT-Unequal Power Dividers for High-Power Division Ratios and Design Methods for Arbitrary Phase Differences," IEEE Trans. MTT, vol. 62, no. 12, Dec. 2014, pp. 2954-2964.

[23] B. Ravelo, B. Mirkhaydarov, G. P. Rigas, M. Shkunov, S. Swaisaenyakorn and P. R. Young, "Design of 5GHz Switched Power Splitter on Organic Flexible Substrate", Proc. of IEEE Int. Wireless Symp. (IWS) 2015, Shenzhen, China, 30 Mar. - 1 Apr. 2015, pp. 1-4.

[24] T. Eudes, B. Ravelo and A. Louis, "Experimental Validations of a Simple PCB Interconnect Model for High-Rate Signal Integrity," IEEE Trans. EMC, vol. 54, no. 2, Apr. 2012, pp. 397-404.